atmosphere

MDPI

Article

Response of Sea Surface Temperature and Chlorophyll-a to Typhoon Lekima (2019)

Yaowei Shi [1], Biyun Guo [1,2,*], Yuqian Niu [3,4], Venkata Subrahmanyam Mantravadi [5,*], Jushang Wang [1], Zhaokang Ji [1], Yingliang Che [1] and Menglu Ye [1]

1 Marine Science and Technology College, Zhejiang Ocean University, Zhoushan 316022, China
2 State Key Laboratory of Hydroscience and Engineering, Tsinghua University, Beijing 100084, China
3 Ocean College, Zhejiang University, Zhoushan 316022, China
4 State Key Laboratory of Satellite Ocean Environment Dynamics, Second Institute of Oceanography, Ministry of Natural Resources, Hangzhou 310012, China
5 School of Marine Science and Technology, Hainan Tropical Ocean University, Sanya 572022, China
* Correspondence: biyunguo@zjou.edu.cn (B.G.); mvsm.au@gmail.com (V.S.M.)

Abstract: Typhoon (hurricane) is the most influential process of ocean–air interaction on the synoptic scale; it has a great influence on the heat exchange, mixing and ecological processes in the upper ocean, which in turn affect sea surface temperature (SST), leading to chlorophyll-a (Chl-a) concentration variation. SST is also an important factor affecting marine fishery resources. Chl-a is closely related to the marine ecosystem and primary productivity. In this study, we analyzed the response of SST and Chl-a to Typhoon Lekima (2019) process. The result indicates that the response of temperature to typhoon decreases from the center to the outer edge, which has a good correlation with the location, path and influence area of the typhoon center. The mean SST in the study area (14°~40° N, 116°~136° E) decreased during the typhoon's passage, from 28.97 °C at the beginning (5 August) to 28.22 °C (15 August). The concentration of Chl-a was high in the northwest and coastal areas; its mean value in the study area decreased from 2 to 8 August (on 2 and 8 August, the concentration was 0.484 mg/m^3 and 0.405 mg/m^3, respectively). From 8 to 14 August, Chl-a decreased with the increase in SST, and 10 and 14 August were the two peak values of Chl-a (while SST was low). Chl-a concentration increased after the typhoon's landfall (from 15 to 31 August); the Chl-a trend was the same as that of SST. The stronger the typhoon and the longer the residence time, the greater the contribution to the increase in Chl-a concentration at sea surface. Typhoon-induced rainfall over the ocean surface, increased evaporation of seawater, enhanced mixing within the mixed layer and upwelling of the pycnocline resulted in an increase in Chl-a quantity. This study describes the spatial response of the upper ocean to typhoons. It provides a general method for the comprehensive assessment of typhoons in marginal seas and upper open oceans, which has wide applicability and good scientific application prospects.

Keywords: typhoon Lekima; SST; chlorophyll-a concentration; wind

Citation: Shi, Y.; Guo, B.; Niu, Y.; Mantravadi, V.S.; Wang, J.; Ji, Z.; Che, Y.; Ye, M. Response of Sea Surface Temperature and Chlorophyll-a to Typhoon Lekima (2019). *Atmosphere* **2024**, *15*, 919. https://doi.org/10.3390/atmos15080919

Academic Editors: Anthony R. Lupo and Yubin Li

Received: 11 May 2024
Revised: 23 June 2024
Accepted: 29 July 2024
Published: 31 July 2024

1. Introduction

In the past few decades, typhoon frequency and intensity have increased, and its translation speed has slowed down [1], which has a significant impact on the regional marine environment. When a typhoon passes, the sea surface wind increases, and the mixing intensifies; therefore, the mixing layer usually deepens [2]. The cyclonic wind stress on the sea surface caused by the typhoon will lead to the upwelling of the lower seawater within a radius of several kilometers, resulting in the uplift of the thermocline [3]. The change in the thermocline will last for several inertial oscillation cycles after the typhoon [4]. After the typhoon, the heat flux from the ocean to the atmosphere is as high as 100 W/m^2, and there is a cooling process in the ocean mixing layer, which makes the temperature of the surface mixing layer drop by 1 °C on average [5,6]. The influence of typhoon on the

ocean can exceed 1000 m depth; the temperature decreases with depth, the stratification is obvious at depth, and the exchange is weak at the bottom [7–11]. The stratification of temperature hindered the transport of nutrients from the lower layer to the mixing layer, resulting in lower nutrients in the surface layer and higher Chl-a concentration in the lower layer [12]. Typhoon caused strong mixing of seawater, bringing the lower layer cold water to the surface layer [13]. The spatial distribution of Chl-a depends on the relationship among the thickness of the mixed layer, the trophic thermocline and the maximum Chl-a concentration in the lower layer [12].

The responses of Chl-a and SST to typhoons are very different both in space and between single typhoon events [14]. Typhoon Lekima formed on 4 August 2019. In this study, the response of SST and Chl-a around the track of Lekima to the typhoon process was studied. Chl-a is important for the study of primary productivity in the marine ecosystem, which provides an important basis for the study of carbon cycle in the marine atmospheric system and global heat effect circulation, and it is of great significance for the study of ocean current (upwelling, coastal current, etc.) and marine fishery management [15–17]. Satellite remote-sensing data (such as MODIS, SeaWiFS, Goci, MERIS, etc.) have high spatial-temporal resolution [7] and can be used for large-area synchronous observation; therefore, they are widely used in marine Chl-a concentration estimation and spatial-temporal dynamic analysis [15–17]. SST combined with other remote-sensing data, such as chlorophyll a, wind field and sea surface height, has increasingly become an important data source in oceanographic research, especially in severe weather conditions, such as typhoons. Due to the severe weather of typhoon, it is difficult to measure the condition of the ocean by conventional methods.

The development of remote-sensing technology provides an effective means for the study of such extreme events. There are many studies on the use of satellite data to detect the ocean surface characteristics over the area of typhoon passage, while there are few studies on the Chl-a concentration, temperature and the relationship between them before and after the typhoon [18–21]. In this study, remote-sensing technology was used to study the temporal and spatial variations in Chl-a concentration and temperature in the sea area where Lekima (Typhoon No. 9 in 2019) passed through.

2. Materials

The study site is the sea area around Typhoon Lekima path, with a range of 14°~40° N, 116°~136° E (Figure 1). The data used in this study include wind, sea surface temperature (SST) and chlorophyll-a (Chl-a). The wind, sea surface temperature (SST), Chl-a and Ekman pumping velocity (EPV) were analyzed using MATLAB R2023a software.

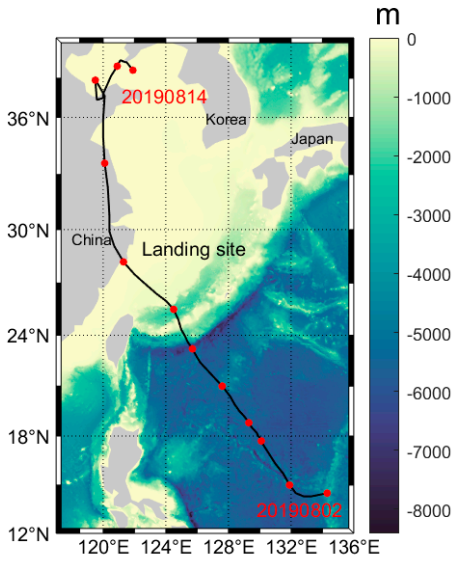

Figure 1. The route of Typhoon Lekima No. 9 in 2019.

2.1. The Overview of Typhoon Lekima No. 9 in 2019 [22,23]

On the afternoon of 30 July 2019, a tropical disturbance formed over the eastern waters of the Philippines. On the afternoon of 3 August, this developed to a tropical depression. On the afternoon of 4 August, the tropical depression officially strengthened to Lekima, the ninth typhoon of the year, and strengthened to super typhoon status at 23:00 on 7 August (Beijing time, the same below). It landed in Chengnan Town, Wenling City, Taizhou City, Zhejiang Province, China, on 10 August at 01:45, ranking as the third strongest typhoon landing in Zhejiang since the founding of the People's Republic of China (the intensity of landing was a super typhoon, and the maximum wind speed near the center was 52 m/s, level 16). After landing, the intensity gradually weakened, passing through Zhejiang and Jiangsu Province and then moving northward through the Yellow Sea. At 20:50 on 11 August, it made a second landing in the coastal area of Huangdao District, Qingdao City, Shandong Province, and then dissipated in the Bohai Sea, with a life span of 9 days. The specific path is shown in Figure 1. In Figure 1, the black line from the southeast to the northwest is the track of Typhoon Lekima.

The black line represents Lekima's path, and the red dot represents the typhoon center.

From 08:00 on 8 August to 08:00 on 11 August, the average rainfall in Zhejiang Province was 165 mm. There are mainly two heavy rainfall areas: one is located near the typhoon center, and the other is located in the area from the north of Taizhou to the south of Ningbo. In addition, there are some heavy rainfalls in the northwest of Zhejiang Province. In Taizhou, the typhoon landed in 9 counties (cities, districts); there were 5 areas with rainfall exceeding 300 mm; and the maximum rainfall was 370.9 mm in Huangyan District. The maximum precipitation measured by a single station was Kuocangshan station in Linhai City, and the accumulated precipitation during the process was 834.3 mm. The maximum hourly rainfall intensity was 896.6 mm in Ximen island of Yueqing, Wenzhou City.

2.2. Wind

Wind data were acquired from the dataset of the Navy Global Environmental Model (NAVGEM), which is a global numerical weather prediction computer model run by NOAA. In mid-February 2013, it replaced NOGAPS as the primary model for FNMOC weather model weather sites. NOGAPS is the global weather forecast model from the "Fleet Numerical Meteorology and Oceanography Center" (USA). It is located 10 m above the sea surface (spatial resolution of 1 degree) and is provided by the Navy Fleet Numerical Meteorology and Oceanography Center (FNMOC). This study period is from 3 August to 12 August 2019 (https://coastwatch.pfeg.noaa.gov/erddap/griddap/erdNavgem1D10mWind_LonPM180.html, accessed on 22 June 2024).

2.3. Sea Surface Temperature (SST)

The study period is from 1 July to 31 August 2019. The SST used in this study is from the dataset of Advanced Very High-Resolution Radiometer (AVHRR) Pathfinder Version 5.3 Level 3-Collated (L3C) SST, global, 0.0417°, daytime (1 Day Composite), provided by the National Centers for Environmental Information, USA. This is a retrospectively processed skin-level SST dataset available from 1981 to the present for climatological application [24]. This dataset comprises twice-daily (day/night) data, which are generated with measurements combined from a single AVHRR instrument (at a time) into a space-time grid. Thus, a dataset for time is a combination of multiple channels/scenes grouped together (https://coastwatch.pfeg.noaa.gov/erddap/griddap/nceiPH53sstd1day.html, accessed on 22 June 2024).

2.4. Chl-a

The data used for this study are from the typhoon period. The daily Chl-a concentration was obtained from the National Oceanic and Atmospheric Administration (NOAA) Coast Watch. The NOAA Multi-Sensor Level-1 to Level-2 (MSL12) Ocean Color, with quality science, multi-sensor global gap-filled analysis, includes Chl-a products. The data gaps

were generated by using the data interpolating empirical orthogonal function (DINEOF) method [25]. The data currently come from 3 instruments: the Visible Infrared Imaging Radiometer Suite (VIIRS) sensor (aboard the Suomi National Polar-Orbiting Partnership Satellite), the VIIRS on the NOAA-20 satellite and the Ocean and Land Color Instrument (OLCI). The level 3 Chl-a (mass concentration) data over the sea surface used for this study have a spatial resolution of 4 km and are obtained daily from the National Oceanic and Atmospheric Administration (NOAA) Coast Watch/Ocean Watch. The data obtained for this study period are from August 2019.

Light reflected from or transmitted through a volume of water can be measured on a large scale to determine the average or mean influence of particles interacting with the light field; the approaches to characterizing the individual particle's size and optical characteristics show heterogeneity that is not addressed by large-scale or bulk measurements; it is typically not appropriate to determine the average properties of a whole volume solely on the average properties of individual particles or elements in the medium because most biological optical processes are non-linear [26]. The model needs to take this heterogeneity into account in a rigorously mathematical manner to link observations taken at different scales [27]. Logarithmic transformations are frequently employed when working with data that are obviously not regularly distributed, particularly in the biological and optical sciences; for bio-optical variability over a range of space-time scales, the lognormal model is helpful; these kinds of data can be analyzed using a rigorous statistical framework that the lognormal model offers; since log-converted bio-optical data tend to be normally distributed in many circumstances, the technique was based on the lognormal distribution [28]. Because the value range of sea surface Chl-a is large, it is not convenient for cartographic analysis; therefore, it is standardized (its logarithm is calculated) to achieve the compression range and facilitate the analysis of its temporal and spatial changes (https://coastwatch.star.nesdis.noaa.gov/pub/socd1/mecb/coastwatch/viirs/science/L3/global/chlora/dineof/2019/, accessed on 22 June 2024).

2.5. Ekman Pumping Velocity (EPV)

Ekman pumping refers to the convergence (divergence) of air at the top of the Ekman layer due to turbulent friction. The Ekman pumping effect enhances the exchange of momentum, heat and water vapor between the free atmosphere and the boundary layer [29]. The Ekman pumping velocity (EPV) is calculated from the wind stress and Coriolis parameters by using Climate Data Toolbox for MATLAB [1,30–32]. The formula is shown in Equation (1) [2]:

$$W_{EK} = (\text{curl } \tau)\ (\rho\ f) \quad (1)$$

In Formula (1), W_{EK} represents the EPV (m/s); τ is the surface wind stress (N); ρ is the seawater density (1025 kg/m^3); f is the Coriolis parameter (=2Ω sin θ, Ω and θ are the angular velocity and latitude of the earth, respectively). The calculation method of surface wind stress is shown in Equation (2) [1]:

$$T = [\tau_x, \tau_y] = \rho_a\ C_D\ V\ [u, v] \quad (2)$$

In Formula (2), τ_x and τ_y represent the east–west and north–south components of wind stress (N); ρ_a is the density of sea surface air; C_D is the drag coefficient; V [u, v] is the wind speed (m/s); and u and v are the east–west and north–south components of wind speed.

3. Results

3.1. Wind Variation during the Movement of Typhoon Lekima

Lekima formed in the northwest Pacific Ocean and dissipated over the Bohai Sea [23]. It had the characteristics of "strong landing intensity, long land retention time and wide impact area", which caused serious casualties and economic losses to many coastal provinces of China [22].

The wind is measured at 10 m above sea level with a spatial resolution of 1 degree and a temporal resolution of 6 h; the period is between 3 and 12 August 2019. The vector average analysis of the daily wind speed and direction in the passing area during the typhoon is carried out by using MATLAB software (see Figures 2 and 3). Figure 2 illustrates the variation in wind speed and direction in the area affected by the typhoon. The blue line indicates the typhoon path; the red dots represent the typhoon center; and the vectors (in black) represent wind direction and speed. Figure 3 shows the spatial distribution of wind speed; the transition from blue to red indicates that the wind speed increases from low to high. From 3 to 12 August, the typhoons experienced formation, strengthening and extinction. The wind speed is high in the area around the typhoon. In Figure 3, yellow or red-orange is the location of the typhoon center (from 3 to 12 August; some areas in the southeast from 10 to 12 August, which is the strong wind area affected by Typhoon Krosa No. 10, 2019). As the typhoon approaches closer to the center, the wind speed will be higher, and the wind direction will be counterclockwise.

3.2. SST Changes during Typhoon Lekima's Passage

In a large-scale air–sea interaction, the effect of the atmosphere on the ocean is mainly dynamic, while the effect of the ocean on the atmosphere is mainly thermal. SST represents the comprehensive results of ocean thermal and dynamic processes and the interaction between the ocean and the atmosphere [33]. SST is an important parameter, reflecting the heat, dynamic and water vapor exchange between the sea and air, and it is an important factor affecting climate change, marine nutrient concentration and primary productivity. In recent years, tropical storms have become more and more intense, which is closely related to the rise in ocean temperature [34].

Typhoon Lekima, which formed at 17:00 (Beijing time) on 4 August, became a strong tropical storm at 02:00 on 6 August, evolved into a typhoon at 05:00 on 7 August, strengthened into a strong typhoon at 17:00 and became a super typhoon at 23:00 on 7 August, and landfall occurred in Zhejiang Province at 01:00 on 10 August. In the process of typhoon formation and evolution, the regional temperature changed a lot. In the area where the typhoon passes, the SST decreases to varying degrees. The changes in the ocean and atmosphere are coupled as a whole, not isolated from each other. MATLAB software was used to analyze the spatial changes in SST during Lekima (from 3 to 12 August) and the changes in daily mean SST in the study area in August. The results are shown in Figures 4 and 5.

Figure 4 shows the spatial (14°~40° N, 116°~136° E) variation in SST before and after Lekima. In Figure 4, the white solid line is the path that the typhoon had passed; the red dotted line is the path that the typhoon will pass; and the black dot is the typhoon center. The SST change in the typhoon-affected area is obvious. In Figure 4, the temperature in the area near to the typhoon's path dropped significantly from 6 to 12 August. Before Lekima (3 August), the SST in most parts of the north (32°~40° N) was lower than 28.3 °C; however, in most parts of the middle and south (14°~32° N), the SST was higher than this. On 4 August, the SST in most of the area was in the range of 28.8~30.0 °C (14°~40° N, 116°~136° E); when Lekima passed through, the SST dropped significantly after 5 August, especially in the track area of Lekima. From 6 August, a low SST zone (around 28 °C) appeared on both sides of the typhoon track, and then, the low temperature zone gradually expanded. SST gradually increased until 15 August; however, it was still lower than before the typhoon had passed through. Another phenomenon is that as the typhoon moves forward, the SST in the early track area gradually rises.

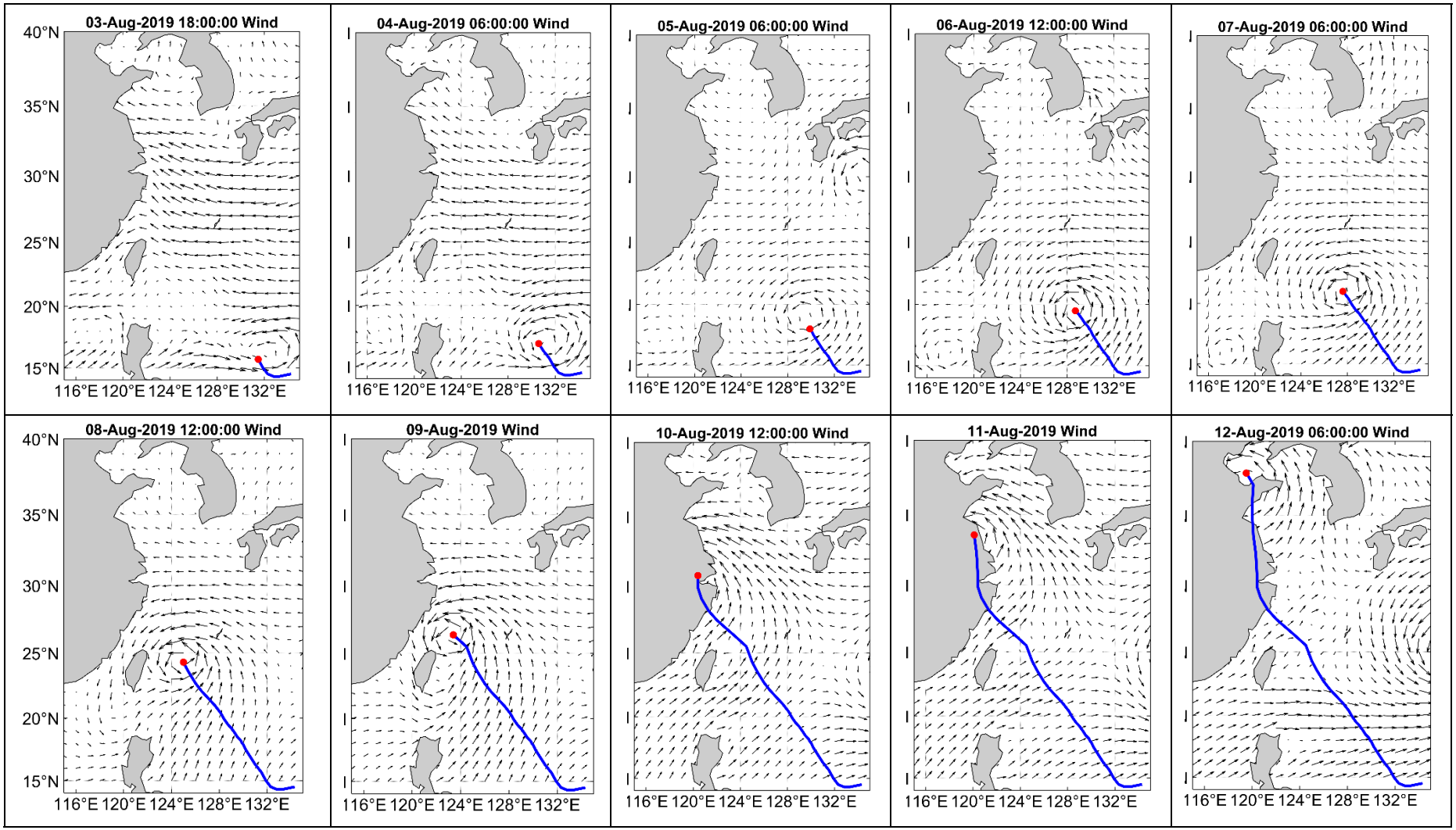

Figure 2. Wind direction and track of Typhoon Lekima. The blue line is the typhoon path; the red dot is the typhoon center; and the black arrow is the wind direction and speed (long arrows have higher wind speed and vice versa).

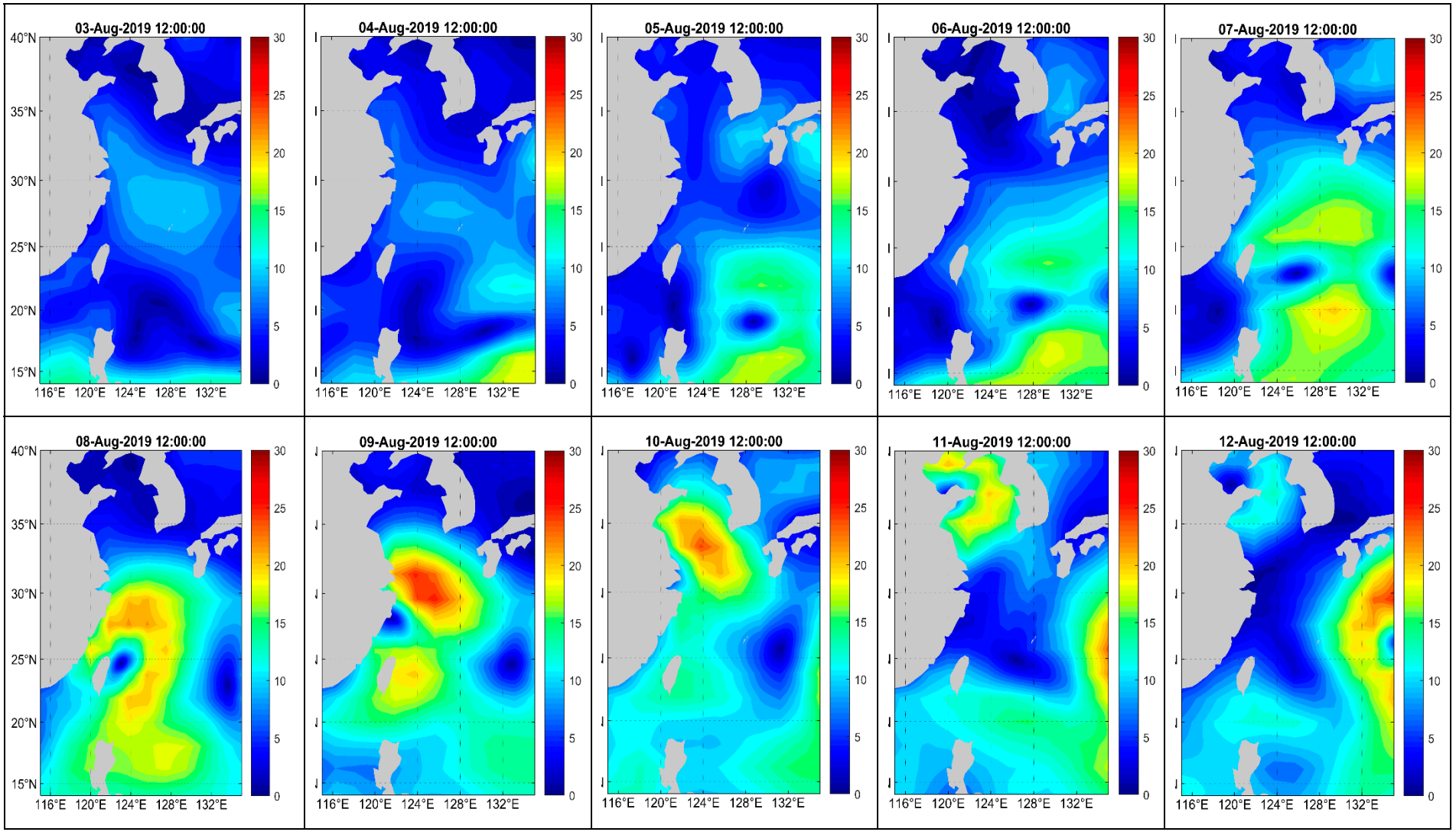

Figure 3. Wind speed during Typhoon Lekima's passage. Unit: m/s. The transition from blue to red indicates an increase in wind speed from low to high.

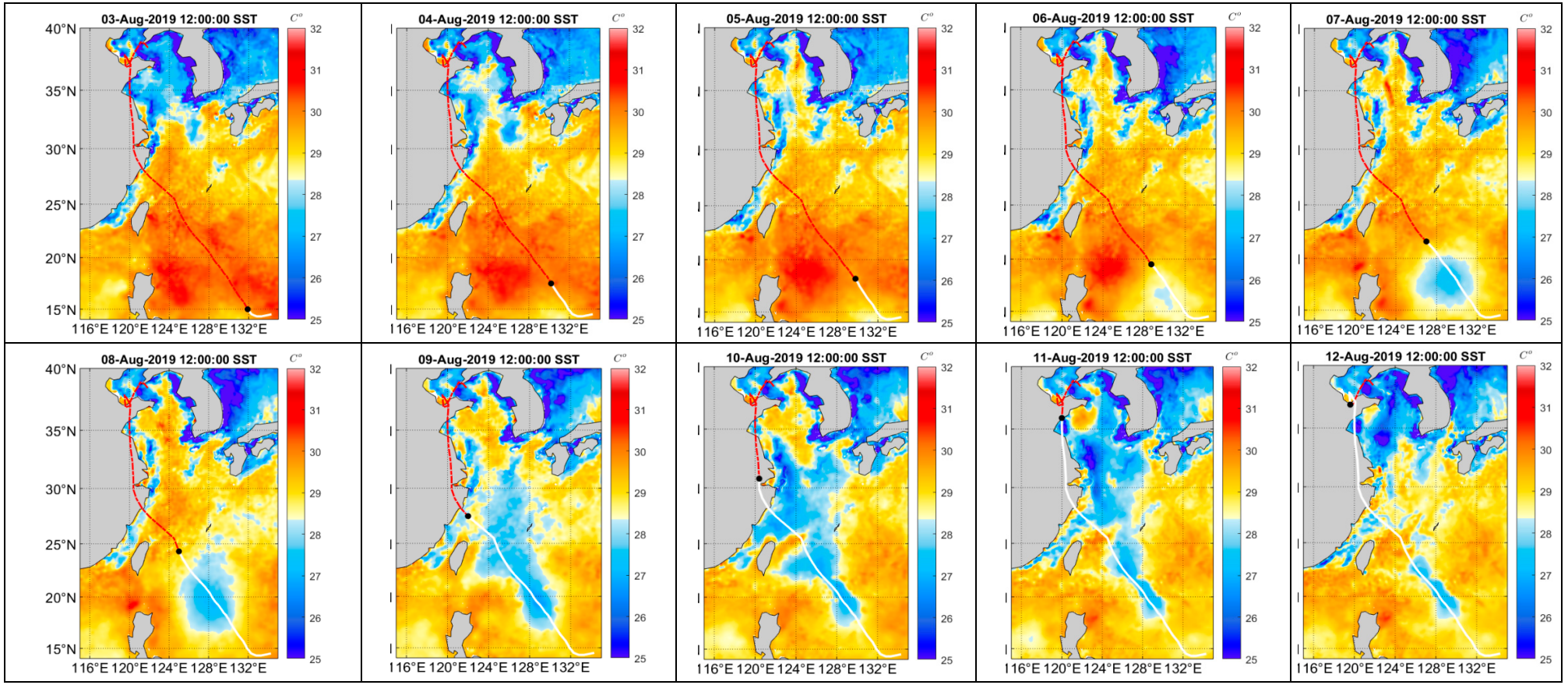

Figure 4. The temperature changes around the track of the typhoon before and after its passage. The line from the southeast to the northwest is the path of Typhoon Lekima. White represents the track that the typhoon had passed, and red represents the track that the typhoon will pass. The black dot is the typhoon center.

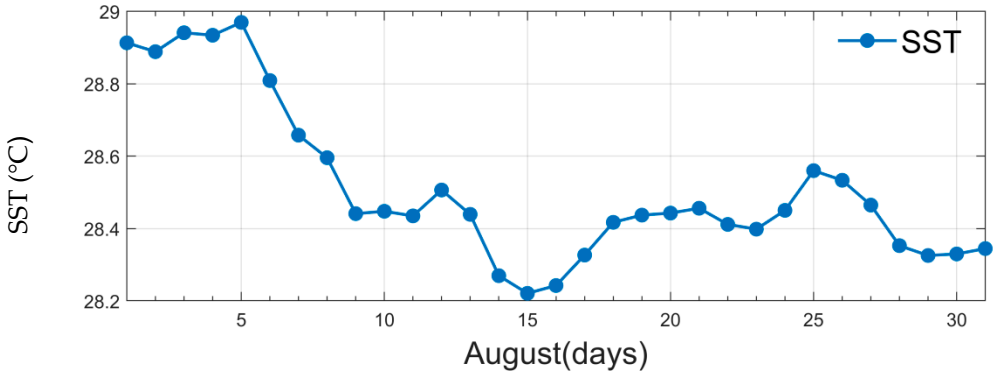

Figure 5. Changes in daily mean SST over the passage of Lekima from 1 to 31 August 2019.

Figure 5 shows the daily mean SST in the area (14°~40° N, 116°~136° E), which was affected by Lekima in August 2019; the mean monthly SST was 28.5 °C in August. From 1 to 5 August, the daily mean SST was higher than 28.89 °C, and the maximum was 28.97 °C on 5 August. With the strengthening of Lekima, the daily mean SST decreased from 28.97 °C (5 August) to 28.22 °C (15 August). After 15 August, the SST increased slightly. The SST drop is due to the increase in wind and seawater mixing when the typhoon passes, and strengthened wind can cause the deepening of the mixing layer [35]. The cyclonic wind stress on the sea surface triggered will cause the upwelling of the cold seawater in the lower layer within a radius of hundreds of kilometers, resulting in the uplift of the thermocline. Such changes in the thermocline will last for several inertial shock cycles after typhoons [21,22]. The daily mean SST in the study area dropped 0.75 °C during Lekima's passage (see Figure 5). The typhoon not only affects the SST but also the Chl-a in the seawater.

3.3. EPV Changes during Typhoon Lekima's Passage

Based on the hourly wind speed at 10 m sea surface, the EPV and its spatial distribution before and after the typhoon were calculated by MATLAB according to Formulae (1) and (2). The EPV spatial variations (14°~40° N, 116°~136° E) during Typhoon Lekima are given in Figure 6. A positive EPV value indicates an upward flow, while a negative EPV value indicates a downward flow (see Figure 6). The EPV over the ocean can clearly be seen in the figures around the typhoon. However, when the typhoon reaches the coast, the EPV is clearly seen along the coast on the right side of the typhoon, which is due to typhoon winds. When the typhoon made the landfall, the wind pattern changed, as well as the EPV, on 10 August; however the EPV disappeared on 12 August.

When a typhoon passes through, a strong wind stress acts on the upper ocean, causing strong vertical mixing in the upper ocean to deepen the depth of the mixing layer. Upwelling and downwelling caused by the convergence and divergence of mixed layer waters are the main dynamic processes of the ocean. In this paper, the EPV during the transit of Typhoon Lekima is calculated according to Formulae (1) and (2) based on wind field data acquired 10 m from the sea surface. The EPV is proportional to the wind speed in Formulae (1) and (2). Table 1 shows the maximum, average and minimum values of EPV during typhoon transit. The maximum value (positive value) indicates the upward direction of Ekman suction; the minimum value (negative value) indicates the downward direction of Ekman suction; and the mean value represents the average value of EPV within the study range (14°~40° N, 116°~136° E). On 3 August 2019, the typhoon just entered the country; the cyclone intensity increased; and the EPV increased too. The maximum, average and minimum EPV values were 1.45×10^{-4} m/s, 6.19×10^{-7} m/s and -1.48×10^{-4} m/s, respectively. Afterward, the wind speed gradually increased, and the cyclone intensified. On 8 August 2019, the cyclone intensity was the strongest, and the corresponding maximum, average and minimum values of the EPV were 7.79×10^{-4} m/s, -3.47×10^{-4} m/s and -5.31×10^{-4} m/s, respectively. On 9 August 2019, the cyclone approached the coast

until landfall; the wind speed decreased; and the Ekman suction weakened. On 12 August, the cyclone disappeared, and the corresponding maximum, average and minimum EPV values were 3.43×10^{-4} m/s, 4.40×10^{-7} m/s and -1.51×10^{-4} m/s, respectively.

3.4. The Spatial Variation in Chl-a during Lekima's Passage

MODIS inversion of Chl-a's algorithm is based on the absorption and reflection effects of Chl-a in seawater. Chl-a in water shows a strong absorption effect at 440–490 nm (blue light) and high reflectivity peak at 500–550 nm (green light) [36]. Because green light can reflect the Chl-a of phytoplankton in seawater, the reflectivity of green light band will increase with the increase in Chl-a concentration [37]. The inversion formula of Chl-a concentration is based on the correlation between reflectance and Chl-a concentration in the two bands [38,39]. The formula is based on the logarithmic form of the regression equation, such as Formula 1. This formula is also applicable to Chl retrieval from the coastal zone color scanner (CZCS), ocean color and temperature scanner (OCTS) and MODIS water color remote-sensing data [40]. The coefficients in Formula (1) correspond to different satellites, and the coefficient values are calculated and determined according to the Chl-a concentration measured at fixed points and the reflectance of blue-green bands.

$$log_{10}(chlor\_a) = a_0 + \sum_{i=1}^{4} a_i log_{10}\left(\frac{R_{rs}(\lambda_{blue})}{R_{rs}(\lambda_{green})}\right)^i \quad (3)$$

In Formula (3), $R_{rs}(\lambda_{blue})$ is the higher value of reflectivity in the blue band—that is, the higher value in MODIS Band 9 (λ = 443 nm) or Band 10 (λ = 488 nm); $R_{rs}(\lambda_{green})$ is the reflectivity of the green band—that is, MODIS B and 11 (λ = 550 nm); a_i is the coefficient. $a_0 - a_4$ are 0.242, −2.7423, 1.8017, 0.0015, −1.2280, respectively; these were determined by the NASA Bio-Optical Marine Algorithm Dataset [39].

In most cases, the logarithmic transformation of bio-optical data tends toward normal distribution. The logarithm of Chl-a was normally distributed; Chl-a was converted by log_{10} for drawing and analysis [39]. In this study, the logarithmic transformation of Chl-a concentration was carried out in MATLAB software, as shown in Figure 7 [27,39]. The common logarithm is a monotonically increasing function. Figure 7 is the Chl-a concentration (common logarithm) in the sea surface during Lekima's passage (from 4 to 11 August). The distribution pattern of Chl-a (Figure 7) is different from that of SST. The high values of Chl-a were greater than 0.5 log_{10} mg/m^3, which were found near the coast, and the lower values were found far offshore. The high value area is 27°~40° N, 120°~128° E, especially in the estuary area of the Yellow River and the Yangtze River (38° N, 119° E; 31° N, 121° E). The red dot in Figure 7 is the typhoon center, and the line is the moving track (the white solid line is the path that the typhoon had passed, and the red dotted line is the path that the typhoon will pass). It can be seen that Chl-a in the nearshore changes significantly before and after the typhoon's passage. Before the typhoon's passage, the Chl-a concentration is low in the nearshore, while it increases significantly after the typhoon passes. On 10 August, Lekima landed in Chengnan Town, Wenling, Taizhou city. On that day, the Chl-a concentration in this area increased significantly compared with the previous value (the value was in the range of 0.5–1.5 log_{10} mg/m^3).

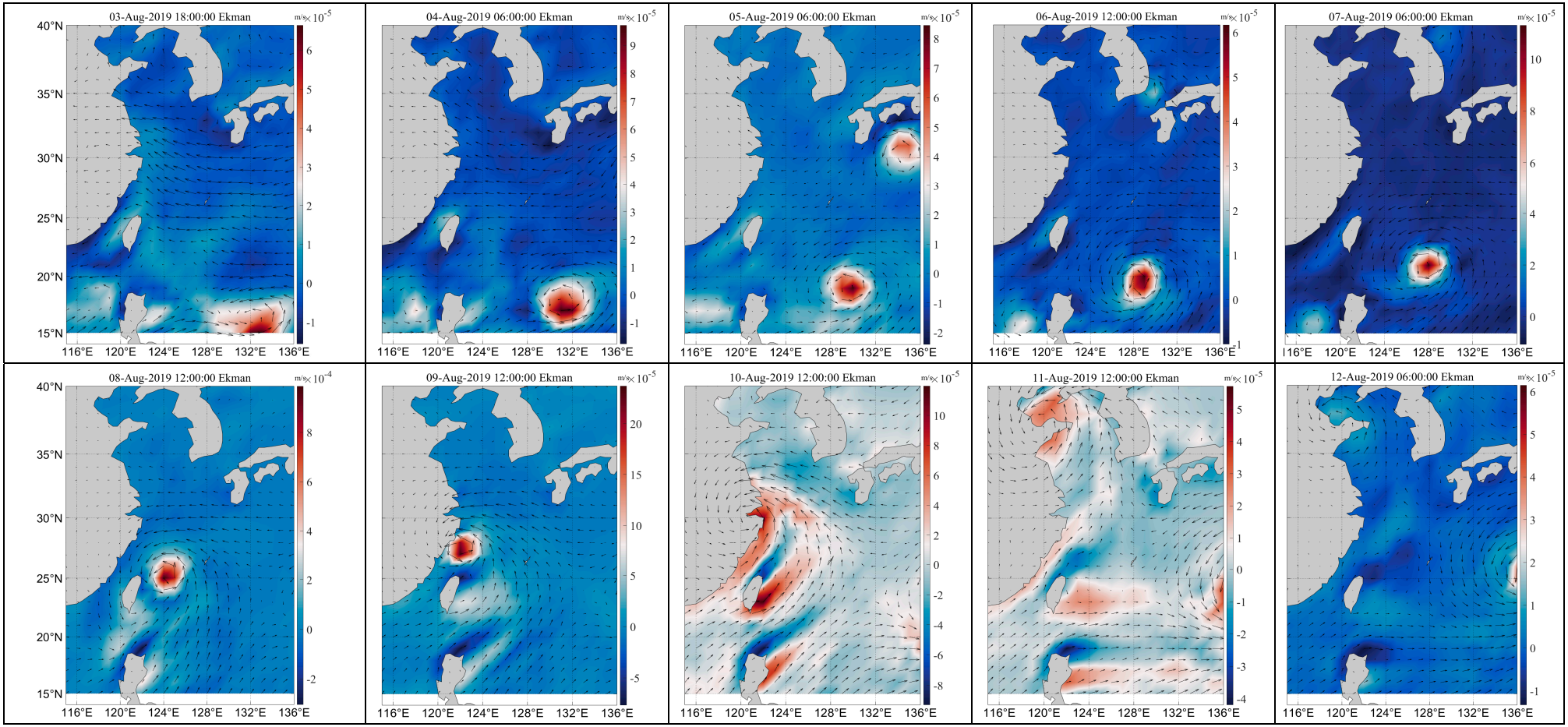

Figure 6. Spatial variation in EPV during Lekima's passage (2019). The direction of the arrow represents the wind direction, and the length represents the wind speed. The background color ranges from blue to red, indicating a gradual increase in wind speed.

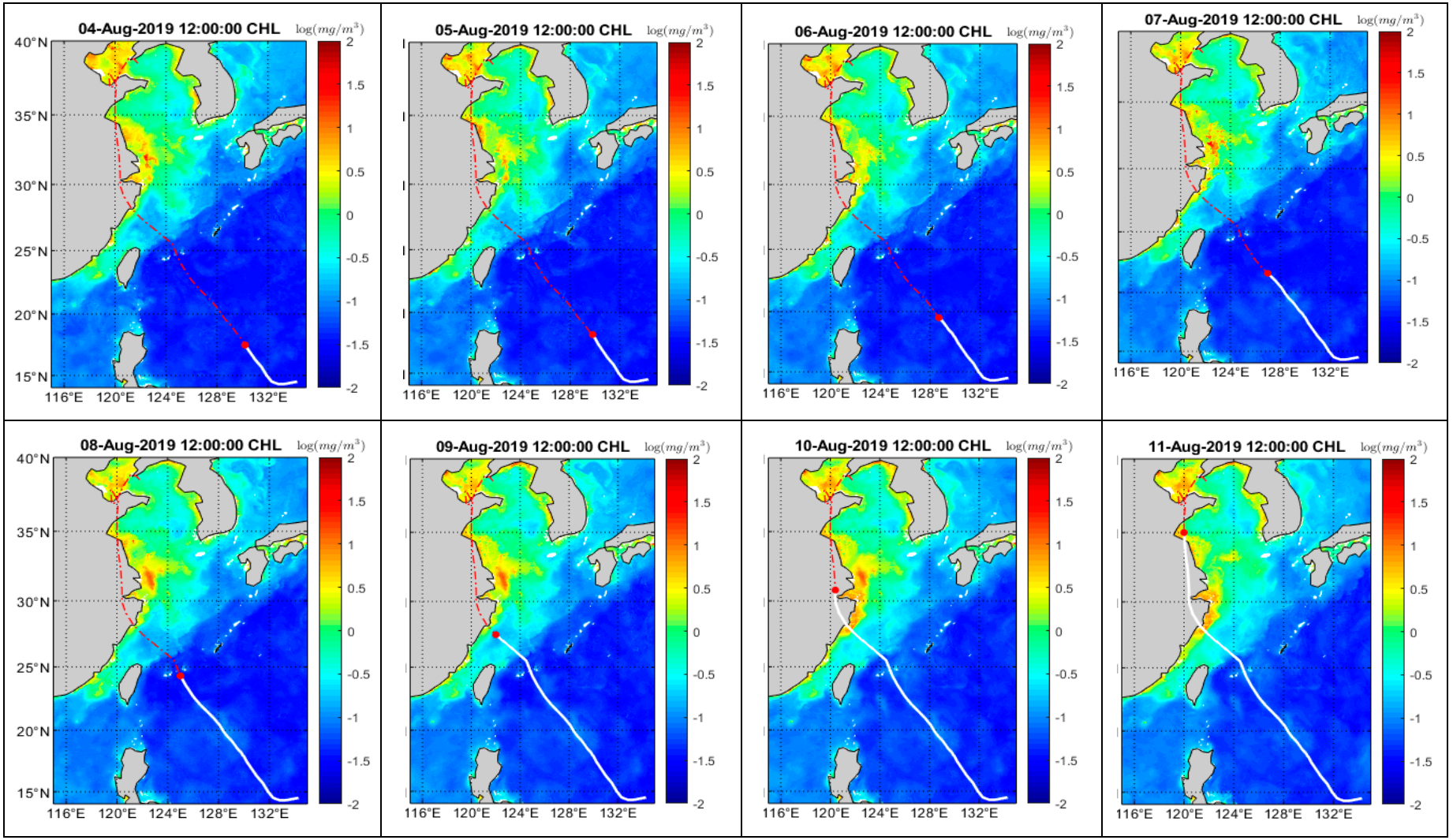

Figure 7. Spatial and temporal distribution of sea surface Chl-a concentration during Lekima's passage. Chl-a was converted to a logarithmic scale. Chl-a (log_{10} (mg/m^3)). The line from the southeast to the northwest is the path of Typhoon Lekima. White represents the track that the typhoon had passed, and red represents the track that the typhoon will pass. The red dot is the typhoon center.

Table 1. Variation in EPV during Lekima's passage (2019).

Time	Maximum (m/s)	Minimum (m/s)	Mean (m/s)
3 August 2019 18:00	1.4463×10^{-4}	-1.4769×10^{-4}	6.1895×10^{-7}
4 August 2019 06:00	1.9781×10^{-4}	-1.1461×10^{-4}	9.9883×10^{-7}
5 August 2019 06:00	1.9332×10^{-5}	-1.8586×10^{-5}	1.0662×10^{-7}
6 August 2019 12:00	5.9190×10^{-5}	-4.6737×10^{-5}	3.3041×10^{-7}
7 August 2019 06:00	1.1307×10^{-4}	-1.2251×10^{-4}	2.0743×10^{-7}
8 August 2019 12:00	7.7927×10^{-4}	-5.3071×10^{-4}	-3.4666×10^{-6}
9 August 2019 12:00	2.3698×10^{-4}	-1.3785×10^{-4}	-1.5624×10^{-6}
10 August 2019 12:00	1.5550×10^{-4}	-1.5578×10^{-4}	-6.4482×10^{-8}
11 August 2019 18:00	2.2333×10^{-4}	-6.3961×10^{-5}	1.3612×10^{-6}
12 August 2019 18:00	3.4288×10^{-4}	-1.5077×10^{-4}	4.3975×10^{-7}

Maximum, maximum upward EPV in the area. Minimum, maximum downward EPV in the area. Mean, the average EPV in the area.

4. Discussion

Typhoons can affect the ocean's dynamic factors and subsequently cause changes in the ocean's parameters. The decrease in SST and the rise in Chl-a were the main characteristics of the typhoon's passage over the area (Figures 2–4 and 7). This is mainly because the mixing and upwelling caused by typhoons weaken the stratification of the water column [41].

4.1. Response of SST to Typhoon Lekima

After Lekima had passed, there was an obvious low-temperature area around the typhoon's path. A warm sea surface can provide favorable conditions for the upward transportation of heat and water vapor. Under the influence of the typhoon, the temperature in the region (14°~40° N, 116°~136° E) where the typhoon passed decreased by a maximum of 5 °C [42,43]. In the formation and infancy of Lekima (1–5 August), the daily average SST in the study area (14°~40° N, 116°~136° E) was over 28.9 °C; the lowest was 28.2 °C on 15 August, which decreased by 0.7 °C. During the period from Lekima entering the East China Sea to the offshore, the SST was maintained at 28~30 °C, which means that the lower atmosphere over the East China Sea had abundant warm and humid air energy and vigorous sea surface evaporation. This not only ensured the maintenance of the intensity of Lekima before landing but also created favorable conditions for the generation of heavy precipitation. The changes in the ocean and atmosphere during typhoons are a coupled whole rather than isolated from each other. Typhoons receive energy from the ocean, intensify and then act on the ocean, forming large areas of low SST. As the ocean cools, it provides less energy, and the typhoons weaken.

Based on the daily average SST in July and August 2019 in the study area, the spatial distribution of the monthly average SST was calculated. In order to better understand the spatial variation in SST during the typhoon's passage, SST during the typhoon process was compared with the average SST in July and August 2019. The anomalies of SST on each day during Lekima's passage are shown in Figure 8. The figure indicates SST variation in the affected region compared with the mean SST in July and August, and the range of temperature change is approximately 0~5 °C (increase and decrease). Before the typhoon (2–4 August), the SST in the north was 1~2 °C higher than that in the center, south and also on both sides of the typhoon track. As the typhoon progressed (starting on 5 August), the SST in the typhoon path decreased significantly. In the typhoon track area, the maximum cooling range occurred during the arrival of the typhoon and one day later, and SST dropped approximately 1~3 °C; then, SST gradually increased near the typhoon track. From 7 August, there was widespread cooling in the south, with SST dropping approximately 2 °C in the area where the typhoon passed. However, in most northern areas where the typhoon did not pass (such as on 8 August), the SST increased by more than 2 °C. As the center of the typhoon approached (8–14 August), the SST in the northern region dropped from south to north. After Lekima's passage, the SST gradually increased but still kept the temperature lower than before. This shows that SST did not return to the initial state during this period, and the increase in SST took time.

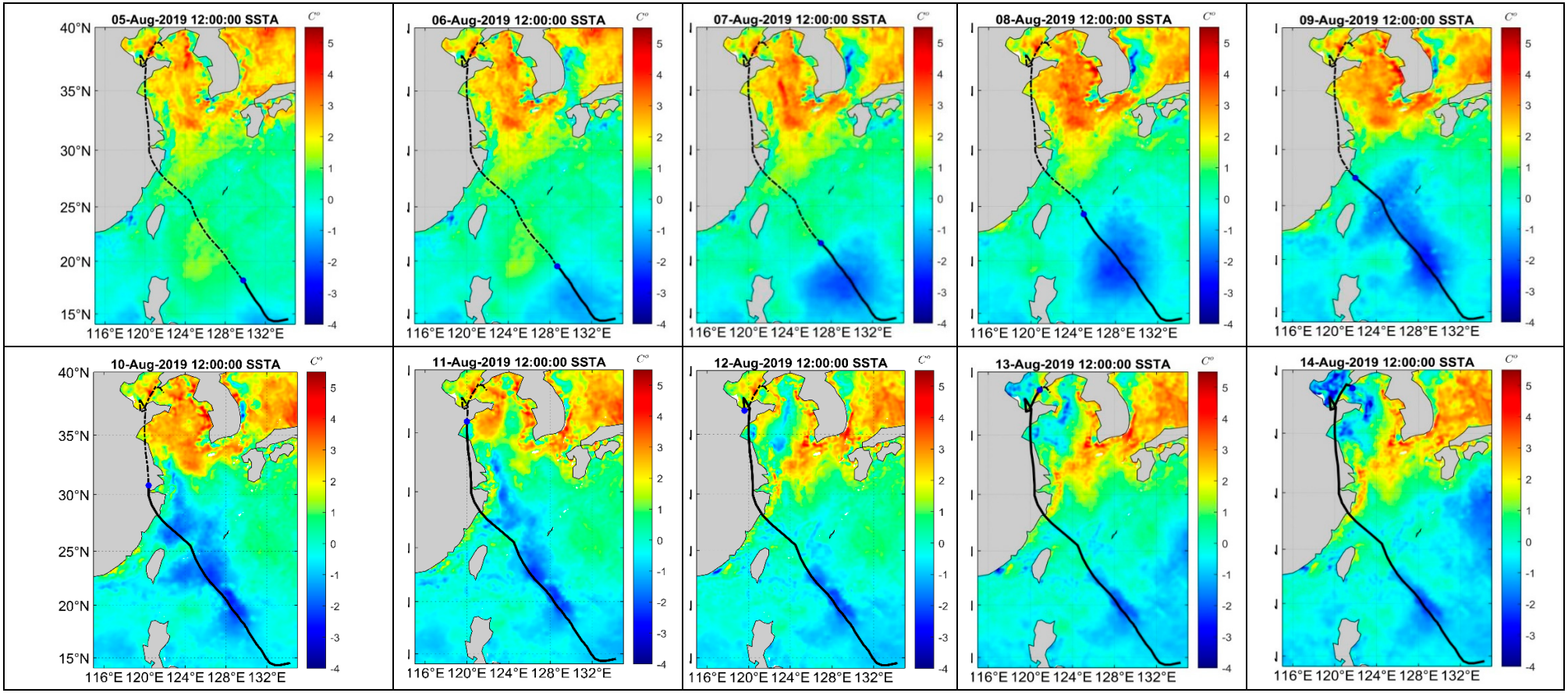

Figure 8. Response of SST to Typhoon Lekima. The line from the southeast to the northwest is the path of Typhoon Lekima. Solid line represents the track that the typhoon had passed, and dotted line represents the track that the typhoon will pass. The blue dot is the typhoon center.

The location of the main low-temperature water region caused by the typhoon basically corresponds to the area with the strongest wind speed (combining Figures 2–4 and 8). The higher the wind speed is, the greater the wind stress will be, and the stronger the mixing that will be generated in the upper ocean. Due to the diffusion effect of ocean currents on the low-temperature zone, this area will be slightly larger. Upwelling, vertical mixing, suction, rainfall, low solar radiation and high latent heat flux are the main causes of sea surface cooling caused by typhoons [4,44]; the stronger the typhoon intensity, the stronger the suction of the ocean [45].

4.2. Response of SST to Typhoon Lekima at Zhejiang Coastal Region

Figure 9 shows the daily mean SST in the area, which was affected by Lekima in August 2019, at Zhejiang coast (115~135° E, 15~35° N). On 1 August, the daily mean SST was 28.9 °C, and the maximum was 29.5 °C on 17 August. With the strengthening of Lekima, the mean SST decreased from 28.97 °C (6 August) to 13.7 °C (9 August). After 6 August, the SST increased. The SST drop is due to the increase in wind and seawater mixing when the typhoon passes. The cyclonic wind stress on the sea surface triggered will cause the upwelling of the cold seawater in the lower layer within a radius of hundreds of kilometers, resulting in the uplift of the thermocline. Such thermocline variations will last for several days after typhoons [21,22]. The average SST in the Zhejiang coastal area dropped 15.2 °C during Lekima's passage over the coastal area (see Figure 9) due to strong upwelling and rainfall, attaining the maximum value on 17 August. The typhoon not only affects SST during passage; it also affects the Chl-a in the seawater after passage.

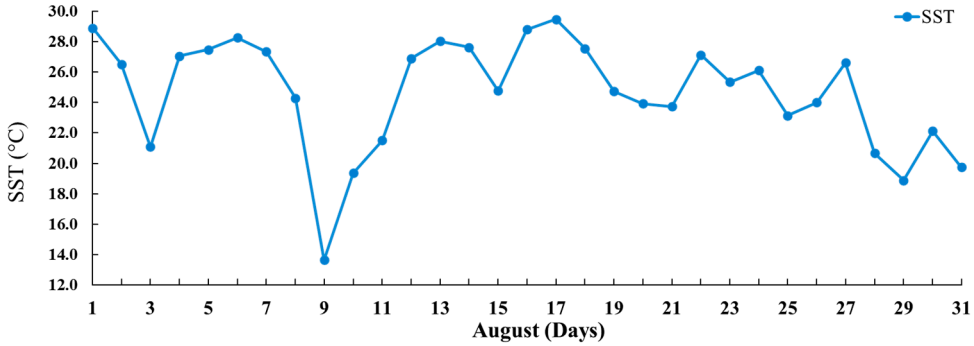

Figure 9. Changes in daily mean SST over the passage of Lekima in Zhejiang coastal area from 1 to 31 August 2019.

4.3. Response of Chl-a to Typhoon Lekima

The variation in Chl-a is influenced by the SST, wind speed and ocean current, etc., and its spatial distribution reflects the large-scale vertical transport of nutrients driven by these factors [46–48]. The upwelling, suction and entrainment caused by typhoons (please refer to Figure 6, where the EPV is located along the coast) bring the nutrients in the subsurface layer to the upper layer and promote the growth of phytoplankton and Chl-a, which has an important impact on the primary productivity and carbon cycle in the oligotrophic sea area [49]. When the EPV is located along the coast, there is upwelling occurring near the coastal areas, and further, the Chl-a increases due to the surface water moving away from the coast and subsurface nutrient water appearing on the surface. The typhoon caused a significant increase in the concentration of Chl-a on the sea surface in the cold-water area, which was related to the bringing of nutrients and biological pigments to the surface and would last for 2~3 weeks before returning to the level before the typhoon [50]. Typhoon enhanced Chl-a and affected the ecosystem mainly by changing nutrient content through vertical mixing and transportation. In addition, typhoon-related rainfall will increase the river flow into the sea and then increase the intensity of land nutrients as input [50]. However, the response of Chl-a to typhoons varies greatly, which depends on water depth, typhoon speed and intensity [51].

Chl-a variation is obvious in the coastal area of Typhoon Lekima's passage (Figure 10, range: 14°–40° N, 116°–136° E). Chl-a in the nearshore is higher than that in the offshore. Chl-a is low before Lekima's passage, while it is high after the typhoon's passage over the coastal area. After the typhoon's passage, there was an obvious increase in Chl-a around the typhoon's path, which increased rapidly in a short time, and the location was consistent with the low-temperature area. Figure 10 indicates the variations in average Chl-a concentration and mean SST over the study area in August 2019. Following Lekima's passage, the mean SST oscillated, while the Chl-a concentration tracked fluctuations in the SST. The change in SST was negatively correlated with the change in Chl- a concentration before and during the typhoon (from 1 to 14 August); however, the Chl-a concentration increased rapidly from 15 August (see Figure 10). As mentioned in the previous work of Fu et al. [52], the Chl-a concentration in coastal waters increased with a lag of 3–6 days. During Typhoon Lekima, the Chl-a increased after 5 days over the coastal areas of Zhejiang. Before the typhoon (2 August), Chl-a reached a peak value (0.48 mg/m^3) and then continued to decline. It reached a trough value (0.40 mg/m^3) on 8 August and increased over the following two days. It reached a peak value (0.45 mg/m^3) on 10 August and increased after 17 August, remaining at a higher value for the next 3 days.

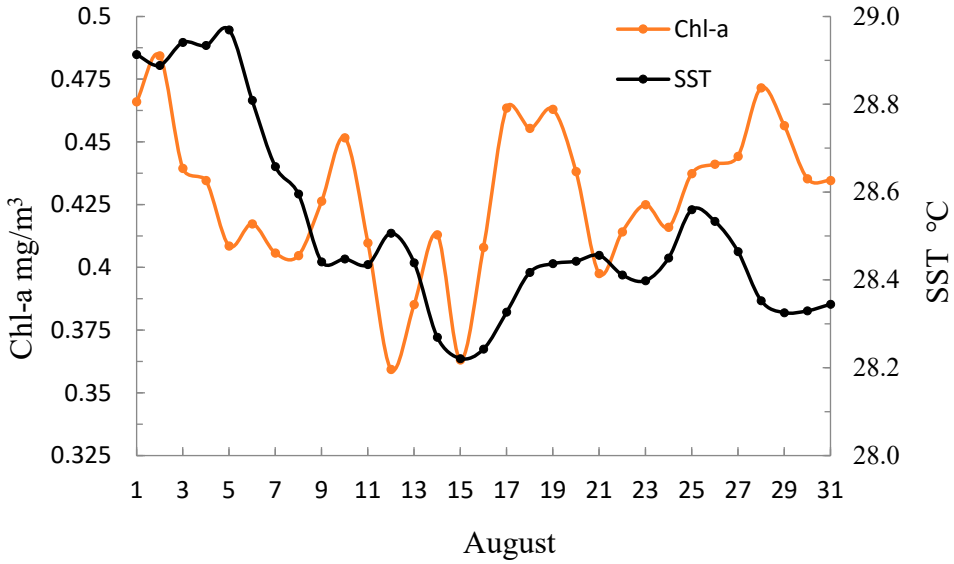

Figure 10. Chl-a concentration variation with SST during Lekima's passage.

After the typhoon, the Chl-a concentration increased significantly in the early typhoon center area (especially in the nearshore; see Figure 7), which was caused by the increase in evaporation, the enhancement of mixing and the upwelling of phytoplankton in the deep layer caused by the upwelling of thermocline. Meanwhile, the surge of cold water in the lower layer brought rich nutrients to the barren upper ocean. In addition, the sunny weather after the typhoon provides favorable conditions for phytoplankton photosynthesis and reproduction, which may also be one of the reasons why the Chl-a concentration exhibited a high value over the next few days. Because the change in the thermocline will last for several inertial cycles after the typhoon, the Chl-a on the ocean surface in the central area will fluctuate with the overall increase after the typhoon. The wind force on the periphery of the typhoon is small, which leads to mixing and thermocline surge being small; therefore, the increase in Chl-a on the periphery of the typhoon is small.

In this study, the error of the Chl-a derived from VIIRS is within 30%, and most Chl-a data are more accurate, such as the median ratio between 0.982 and 1.142 and the median error between 2 and 14% [53].

5. Conclusions

In this paper, we analyzed the impact of Typhoon Lekima on the SST and sea surface Chl-a. Typhoons can affect the ocean dynamically and then cause changes in the ocean's parameters. A decrease in SST and a rise in Chl-a were the main characteristics caused by the typhoon in the study area.

The main reason is that the mixing and upwelling caused by typhoons can attenuate the stratification of the water column [41]. Therefore, as cold and highly nutritious subsurface water rises to the surface, the SST will decrease, and Chl-a will increase [54]. When a typhoon passes by, the surface wind increases, and the mixing intensifies; therefore, it usually causes a deepening of the mixing layer. The cyclonic wind stress on the sea surface caused by typhoons can lead to cold water in the lower layer rising within a radius of hundreds of kilometers, resulting in the uplift of the thermocline [4]. The change in the thermocline will last for several inertial oscillation cycles after the typhoon's passage. After the typhoon's passage, there was a cooling process in the ocean mixing layer, and the temperature of the surface mixing layer decreased by 1 °C on average [55–57].

Typhoon Lekima increased the concentration of Chl-a on the sea surface, which was related to the nutrients and biological pigments being brought to the surface, and this would last for a period of time before returning to normal before the typhoon's passage. The upwelling, entrainment and suction caused by the typhoon bring the phytoplankton in the subsurface and the nutrients in the lower layer to the upper layer, which promotes the growth of phytoplankton and the increase in Chl-a concentration in the sea surface. Heavy rainfall, increased evaporation, enhanced mixing layer and the thermocline surge induced by the typhoon all contributed to the increase in Chl-a to varying degrees. Rainfall caused by typhoons will increase the river flow and then increase the intensity of nutrient input on land [50], which will also affect the distribution of chlorophyll near the shore. When Lekima passed through, the heavy rainfall caused land runoff and offshore flow, which carried a large amount of suspended matter, phytoplankton and dissolved organic matter into the sea, forming a higher chlorophyll area in the nearshore. This is also the reason for an increase in Chl-a concentration in the nearshore after a typhoon. Areas near the typhoon track illustrate obvious changes after the typhoon passes; the temperature decreases, and the nutrients and Chl-a increase. The response of Chl-a generally occurs later than that of the SST because the growth of phytoplankton takes several days.

Author Contributions: Conceptualization, B.G., Y.S. and V.S.M.; methodology, Y.S. and B.G.; software, Y.N., J.W., Z.J., Y.C. and M.Y.; validation, B.G. and V.S.M.; resources, V.S.M., J.W., Y.N. and M.Y.; data curation, V.S.M. and Y.N.; writing—original draft preparation, Y.S. and B.G.; writing—review and editing, Y.S., B.G. and V.S.M.; project administration, B.G.; funding acquisition, B.G. All authors have read and agreed to the published version of the manuscript.

Funding: This research was funded by the Consultation and Evaluation Program of the Department of Chinese Academy of Science (2020-ZW11-A-023), the open research fund program of State Key Laboratory of Hydroscience and Engineering, Tsinghua University (sklhse-2021-B-01), Zhejiang Provincial Virtual Simulation Experiment Projects (virtual simulation experimental project for monitoring of suspended sediment in coastal waters using remote sensing), China Scholarship Council (NO. 20230833027), National College Students Innovation and Entrepreneurship Training Program (NO. 202110340039), Zhejiang University Students Science and Technology Innovation Activity Plan (New Talent Program. NO. 2022R411A003), Open Research Fund Program of Key Laboratory for Water Ecology Management and Protection in River Source Areas, Ministry of Water Resources (No. 2024slbjh02) and the National Natural Science Foundation of China (No. 52109092).

Institutional Review Board Statement: Not applicable.

Informed Consent Statement: Not applicable.

Data Availability Statement: Data are contained within the article.

Conflicts of Interest: The authors declare no conflicts of interest.

References

1. Hun, K.S.; Ju, M.I.; Shin, C.P. An increase in global trends of tropical cyclone translation speed since 1982 and its physical causes. *Environ. Res. Lett.* **2020**, *15*, 094084. [CrossRef]
2. Guan, S.; Zhao, W.; Sun, L.; Zhou, C.; Liu, Z.; Hong, X.; Zhang, Y.; Tian, J.; Hou, Y. Tropical cyclone-induced sea surface cooling over the Yellow Sea and Bohai Sea in the 2019 Pacific typhoon season. *J. Mar. Syst.* **2021**, *217*, 103509. [CrossRef]
3. Feng, S.; Li, F.; Li, S. *An Introduction to Marine Science*; Higher Education Press: Beijing, China, 1999.
4. Price, J.F. Upper ocean response to a hurricane. *J. Phys. Oceanogr.* **1981**, *11*, 153–175. [CrossRef]
5. Ioualalen, M.; Wakata, Y.; Kawahara, Y.; Gouriou, Y.; Varillon, D. Variability of the sea surface salinity (SSS) in the Western Tropical Pacific: On the ability of an OGCM to simulate the SSS, and on the sampling of an operating merchant ship SSS network. *J. Oceanogr.* **2003**, *59*, 105–111. [CrossRef]
6. Scoccimarro, E.; Fogli, P.G.; Reed, K.A.; Gualdi, S.; Masina, S.; Navarra, A. Tropical cyclone interaction with the ocean: The role of high-frequency (sub daily) coupled processes. *J. Clim.* **2017**, *30*, 145–162. [CrossRef]
7. Zedler, S.E.; Dickey, T.D.; Doney, S.C.; Price, J.F.; Yu, X.; Mellor, G.L. Analyses and simulations of the upper ocean's response to Hurricane Felix at Bermuda Test bed Mooring site: 13–23 August 1995. *J. Geophys. Res.* **2002**, *107*, 3232. [CrossRef]
8. Xiang, J. *Marine Biology*; Science Press: Beijing, China, 2003.
9. Xu, D.; Liu, Z.; Xu, X.; Xu, J. The influence of typhoon on the sea surface salinity in the warm pool of the western Pacific. *Acta Oceanol. Sin.* **2005**, *27*, 9–15.
10. Kessler, W.S. The circulation of the eastern tropical Pacific: A review. *Prog. Oceanogr.* **2006**, *69*, 181–217. [CrossRef]
11. Hu, D.; Mao, K.; Chen, X.; Zhao, Y.; Li, Y. Composing analysis on upper ocean response to typhoon in the northwest Pacific. *J. Appl. Oceanogr.* **2018**, *37*, 506–513.
12. Walker, N.; Leben, R.R.; Balasubramanian, S. Hurricane forced upwelling and chlorophyll a enhancement within cold core cyclones in the Gulf of Mexico. *Geophys. Res. Lett.* **2005**, *32*, L18610. [CrossRef]
13. Jiang, X.; Zhong, Z.; Liu, C. The effect of typhoon-induced SST cooling on typhoon intensity: The case of Typhoon Chanchu (2006). *Adv. Atmos. Sci.* **2008**, *25*, 1062–1072. [CrossRef]
14. Chen, D.; He, L.; Liu, F.; Yin, K. Effects of typhoon events on chlorophyll and carbon fixation in different regions of the East China Sea. *Estuar. Coast. Shelf Sci.* **2017**, *194*, 229–239. [CrossRef]
15. Chen, C.; Shi, P.; Mao, Q. Satellite remotely-sensed analysis of distribution characters of chlorophyll concentration in South China Sea. *J. Trop. Oceanogr.* **2001**, *20*, 66–70.
16. Shang, S.; Hong, H.; Zhang, C.; Shang, S.; Hu, J. Chl-a distribution feature of Taiwan Straits region in winter, 1998 as observed by SeaWiFS. *Mar. Sci. Bull.* **2001**, *20*, 25–29.
17. Zhao, H.; Qi, Y.; Wang, D.; Wang, W. Study on the features of chlorophyll-a derived from SeaWifs in the South China Sea. *Acta Oceanol. Sin.* **2005**, *27*, 45–52.
18. Veeranjaneyulu, C.; Deo, A.A. Study of upper ocean parameters during passage of tropical cyclones over Indian seas. *Int. J. Remote Sens.* **2019**, *40*, 4683–4723.
19. Kwon, Y.O.; Riser, S.C. *The Ocean Response to the Hurricane and Tropical Storm in North Atlantic during 1997–1999*; School Oceanography, University of Washington: Washington, DC, USA, 2003.
20. D'Asaro, E.A. The ocean boundary layer below Hurricane Dennis. *J. Phys. Oceanogr.* **2003**, *33*, 561–578. [CrossRef]
21. Lin, I.I.; Liu, W.T.; Wu, C.C.; Chiang, J.C.H.; Sui, C.H. Satellite observations of modulation of surface winds by typhoon induced upper ocean cooling. *Geophys. Res. Lett.* **2003**, *30*, 1131. [CrossRef]
22. Zhou, C.; Chen, P.; Yang, S.; Zheng, F.; Yu, H.; Tang, J.; Lu, Y.; Chen, G.; Lu, X.; Zhang, X.; et al. The impact of Typhoon Lekima (2019) on East China: A post event survey in Wenzhou City and Taizhou City. *Front. Earth Sci.* **2022**, *16*, 109–120. [CrossRef]
23. Tang, J.; Fei, J.; Yu, H. Research of super typhoon Lekima: Forecast, observation, numerical simulation and disaster survey. *Front. Earth Sci.* **2022**, *16*, 1–4. [CrossRef]
24. Saha, K.; Zhao, X.; Zhang, H.; Casey, K.S.; Zhang, D.; Baker-Yeboah, S.; Kilpatrick, K.A.; Evans, R.H.; Ryan, T.; Relph, J.M. *AVHRR Pathfinder Version 5.3 Level 3 Collated (L3C) Global 4 km Sea Surface Temperature for 1981-Present, Dataset*; NOAA National Centers for Environmental Information: Asheville, NC, USA, 2018.
25. Wang, Y.; Liu, D. Reconstruction of satellite chlorophyll-a data using a modified DINEOF method: A case study in the Bohai and Yellow seas, China. *Int. J. Remote Sens.* **2014**, *35*, 204–217. [CrossRef]
26. Campbell, J.W. The lognormal distribution as a model for bio-optical variability in the sea. *J. Geophys. Res.* **1995**, *100*, 13237–13254. [CrossRef]
27. Yentsch, C.M.; Campbell, J.W. Phytoplankton growth: Perspectives gained by flow cytometry. *J. Plankton Res.* **1991**, *13* (Suppl. S1), 83–108.
28. Liu, X.; Wang, M. Filling the gaps of missing data in the merged VIIRS SNPP/NOAA-20 ocean color product using the DINEOF method. *Remote Sens.* **2019**, *11*, 178. [CrossRef]
29. Geider, R.J.; Macintyre, H.L.; Kana, T.M. Dynamic model of phytoplankton growth and acclimation: Responses of the balanced growth rate and the chlorophyll a: Carbon ratio to light, nutrient-limitation and temperature. *Mar. Ecol. Prog.* **1997**, *148*, 187–200. [CrossRef]
30. Kessler, W.S. Mean three-dimensional circulation in the northeast tropical Pacific. *J. Phys. Oceanogr.* **2002**, *32*, 2457–2471. [CrossRef]
31. Greene, C.A.; Blankenship, D.D.; Gwyther, D.E.; Silvano, A.; van Wijk, E. Wind causes Totten Ice Shelf melt and acceleration. *Sci. Adv.* **2017**, *3*, e1701681. [CrossRef] [PubMed]

32. Greene, C.A.; Thirumalai, K.; Kearney, K.A.; Delgado, J.M.; Schwanghart, W.; Wolfenbarger, N.S.; Thyng, K.M.; Gwyther, D.E.; Gardner, A.S.; Blankenship, D.D. The climate data toolbox for MATLAB. *Geochem. Geophys. Geosyst.* **2019**, *20*, 3774–3781. [CrossRef]
33. Bao, X.; Wan, X.; Gao, G.; Wu, D. The characteristics of the seasonal variability of the sea surface temperature field in the Bohai Sea, the Huanghai Sea and the East China Sea from AVHRR data. *Acta Oceanol. Sin.* **2002**, *24*, 125–133.
34. Kawai, Y.J.; Kawamura, H. Evaluation of diurnal warming of sea surface temperature using satellite-derived marine meteorological data. *J. Oceanogr.* **2002**, *58*, 805–814. [CrossRef]
35. Price, J.F.; Sanford, T.B.; Forristall, G.Z. Forced stage response to a moving hurricane. *J. Phys. Oceanogr.* **1994**, *24*, 233–260. [CrossRef]
36. O'Reilly, J.E.; Werdell, P.J. Chlorophyll algorithms for ocean color sensors-OC4, OC5 & OC6. *Remote Sens. Environ.* **2019**, *229*, 32–47.
37. Sasaki, H.; Tanaka, A.; Iwataki, M.; Touke, Y.; Siswanto, E.; Tan, C.K.; Ishizaka, J. Optical properties of the red tide in Isahaya Bay, southwestern Japan: Influence of chlorophyll a concentration. *J. Oceanogr.* **2008**, *64*, 511–523. [CrossRef]
38. Tan, S. Radiative Properties of Euphotic Layer and Their Impacts on Satellite Remote Sensing of Ocean Primary Productivity. Doctoral Dissertation, Chinese Academy of Sciences, Beijing, China, 2007. (In Chinese).
39. Siegel, D.; Behrenfeld, M.; Maritorena, S.; McClain, C.; Antoine, D.; Bailey, S.; Bontempi, P.; Boss, E.; Dierssen, H.; Doney, S.; et al. Regional to global assessments of phytoplankton dynamics from the seaWiFS mission. *Remote Sens. Environ.* **2013**, *135*, 77–91. [CrossRef]
40. Werdell, P.J.; Franz, B.A.; Bailey, S.W.; Harding, L.W., Jr.; Feldman, G.C. Approach for the long-term spatial and temporal evaluation of ocean color satellite data products in a coastal environment. *Coast. Ocean. Remote Sens.* **2007**, *6680*, 66800G. [CrossRef]
41. Chiang, T.; Wu, C.; Oey, L. Typhoon Kai-Tak: An ocean's perfect storm. *J. Phys. Oceanogr.* **2011**, *41*, 221–233. [CrossRef]
42. Liu, S.; Zhang, L.; Zhang, X. Characteristics analysis on rapid intensification of typhoon Mujigae (1522) over the offshore area of China. *J. Meteorol. Sci.* **2017**, *37*, 487–496. (In Chinese)
43. Song, P.; Zhong, Z.; Qi, L.; Yuan, S.; Wang, X. A numerical study on the influence of abnormal local sea surface temperature on the track of tropical cyclone. *J. Meteorol. Sci.* **2017**, *37*, 737–747. (In Chinese)
44. Sanford, T.B.; Black, P.G.; Haustein, J.R.; Feeney, J.W.; Forristall, G.Z.; Price, J.F. Ocean response to a hurricane, Part I: Observations. *J. Phys. Oceanogr.* **1987**, *17*, 2065–2083. [CrossRef]
45. Li, L.; Bao, X.; Gao, G. Numerical experiment of SST response to typhoon process in Yellow Sea and Bohai Sea. *Period. Ocean. Univ. China* **2001**, *31*, 165–172.
46. McClain, C.R. A decade of satellite ocean color observations. *Annu. Rev. Mar. Sci.* **2009**, *1*, 19–42. [CrossRef]
47. Sauer, M.J.; Roesler, C.S.; Werdell, P.J.; Barnard, A. Under the hood of satellite empirical chlorophyll a algorithms: Revealing the dependencies of maximum band ratio algorithms on inherent optical properties. *Opt. Express* **2012**, *20*, 20920–20933. [CrossRef] [PubMed]
48. Yoder, J.A.; Kennelly, M.A. Seasonal and ENSO variability in global ocean phytoplankton chlorophyll derived from 4 years of SeaWiFS measurements. *Glob. Biogeochem. Cycles* **2003**, *17*, 1112. [CrossRef]
49. Sathyendranath, S.; Gouveia, A.; Shetye, S.; Ravindran, P.; Platt, T. Biological control of surface temperature in the Arabian Sea. *Nature* **1999**, *349*, 54–56. [CrossRef]
50. Chen, Y.; Tang, D. Remote sensing analysis of impact of typhoon on environment in the sea area South of Hainan Island. *Procedia Environ. Sci.* **2011**, *10 Pt B*, 1621–1629. [CrossRef]
51. Wei, M.; Lien, C.; Lin, I.; Xie, S. Tropical cyclone-induced ocean response: A comparative study of the South China Sea and Tropical Northwest Pacific. *J. Clim.* **2015**, *28*, 5952–5968. [CrossRef]
52. Fu, D.; Pan, D.; Deng, Y.; Zou, J. Quantitative investigation on typhoon impact on chlorophyll a concentration by remote sensing. *Acta Oceanol. Sin.* **2009**, *31*, 46–56.
53. Wang, M.; Liu, X.; Jiang, L.; Son, S. Visible Infrared Imaging Radiometer Suite (VIIRS) Ocean Color Products, Algorithm Theoretical Basis Document (ATBD), Version 1.0, June 2017. Available online: https://www.star.nesdis.noaa.gov/socd/mecb/color/documents/ATBD_VIIRS_OC_v1.0_June2017_f2.pdf (accessed on 22 June 2024).
54. Baibin, S.M.; Carton, J.A.; Dickey, T.D.; Wiggert, J.D. Satellite evidence of hurricane-induced phytoplankton blooms in an oceanic desert. *J. Geophys. Res.* **2004**, *109*, C03043. [CrossRef]
55. Jaimes, B.; Shay, L.K. Near-inertial wave wake of Hurricanes Katrina and Rita over mesoscale oceanic eddies. *J. Phys. Oceanogr.* **2009**, *40*, 1320–1337. [CrossRef]
56. Rao, A.D.; Babu, S.V.; Dube, S.K. Impact of a tropical cyclone on coastal upwelling process. *Nat. Hazards* **2004**, *31*, 415–435. [CrossRef]
57. Wada, A. Numerical simulation of sea surface cooling by a mixed layer model during the passage of Typhoon Rex. *J. Oceanogr.* **2005**, *61*, 41–57. [CrossRef]